

# Dark matter distribution in the universe and ultra-high energy cosmic rays

Pasquale Blasi\*

*\*NASA/Fermilab Astrophysics Center*

**Abstract.** Two of the greatest mysteries of modern physics are the origin of the dark matter in the universe and the nature of the highest energy particles in the cosmic ray spectrum. We discuss here possible direct and indirect connections between these two problems, with particular attention to two cases: in the first we study the local clustering of possible sources of ultra-high energy cosmic rays (UHECRs) driven by the local dark matter overdensity. In the second case we study the possibility that UHECRs are directly generated by the decay of weakly unstable super heavy dark matter.

## INTRODUCTION

Most of our universe is made of a dark elusive component, whose nature is still unknown. This mysterious component dominates the gravitational interactions in our world and determines the distribution of visible matter, that we associate with galaxies, clusters and superclusters of galaxies and their luminous constituents. We know from the measure of the values of cosmological parameters, that most of the dark matter must be of non baryonic nature. This important finding stimulated the blossoming of numerous proposals of new particles, in the context of theories of Grand Unification or extensions of the Standard Model. Some of the possibilities that have been proposed invoke the existence of super heavy particles, with mass comparable with the mass of the inflaton. These particles might be almost stable and contribute the whole of cold dark matter needed to explain cosmological and astrophysical observations. Independent of the nature of dark matter, astrophysical observations of the visible universe allow us to know how dark matter is distributed in space: primordial fluctuations in the density field result today in a structured distribution of the dark and visible components in the universe. Galaxies are part of this clustering, but similar local overdensities can be seen on larger scales, up to a few tens Mpc, where the universe starts being well described by a homogeneous density field.

An apparently unrelated mystery of modern physics is the existence of particles with energy in excess of  $10^{20}$  eV in the cosmic radiation, the so-called ultra high

energy cosmic rays (UHECRs). These particles are thought to be of extragalactic origin, because the galactic magnetic field is unable to confine particles with such energy. As pointed out in the pioneering papers by Greisen [1] and Zatsepin and Kuzmin [2], if the sources are distributed homogeneously in the universe, the process of photopion production off the photons of the cosmic microwave background (CMB) should cause a strong suppression in the spectrum of UHECRs above  $\sim 5 \times 10^{19}$  eV, what is now known as the Greisen-Zatsepin-Kuzmin (GZK) cutoff. Nevertheless we do detect particles with energy much in excess of this cutoff energy, and we have been unable to identify any straightforward astrophysical source in the direction of arrival of these events. Can the two mysteries, of dark matter and UHECRs be related? We discuss here two possible connections: in sections 2 and 3 we explore the consequences that a local clustering of the sources, driven by the corresponding dark matter clustering, have on the observed fluxes of UHECRs, in comparison with the case of homogeneous distribution. The initial prediction by Greisen and Zatsepin and Kuzmin, was in fact derived in the assumption of sources equally distributed in space. It was later shown by Berezhinsky and Grigorieva [3] that a local overdensity by a factor  $\sim 10$  over  $\sim 20$  Mpc would make the problem of the existence of UHECRs less severe. The local density of sources can now be extracted from large catalogs, so that a realistic determination of the density field can finally be used in the calculation of the fluxes of UHECRs. We use here the PSCz and CfA catalogs for the purpose of calculating the density field. The fluxes of UHECRs are calculated numerically by monte-carlo simulations.

In section 4 we consider a direct connection between dark matter and UHECRs, in the case that dark matter is composed of super heavy quasi-stable particles. Particles fulfilling these requirements have been recently discussed in [4–7] [see also J. Ellis (these proceedings)]. We will review here the current situation and stress some consequences of this model on the observable large scale and small scale anisotropies in the arrival directions of UHECRs.

## MEASURING THE GALAXY DENSITY FIELD

In order to determine the effects of the inhomogeneity of the source distribution on the cosmic ray spectrum, we need to measure the galaxy density field, and in particular its dependence on redshift. In general, it may well be that the sources of UHECRs are of some type not directly related to other known objects like galaxies, but we assume here that the sources of UHECRs have a density field that is proportional to that of ordinary galaxies. We follow the approach presented in [8]. The galaxy density field is usually measured by selecting galaxies from an imaging sky survey and taking their redshifts. Almost invariably, the galaxies are selected to be brighter than some limiting flux  $f_{\text{lim}}$  in some band, expressed as an “apparent magnitude”  $m_{\text{lim}} = -2.5 \log_{10}(f_{\text{lim}}/f_0)$ , where  $f_0$  is an arbitrary zero-point. For all (or for some random subsample) of the galaxies brighter than this, their spectra are taken and their redshifts  $z$  are determined.

However, we cannot simply use the raw distribution of redshifts from such a flux-limited survey, regardless of the way the galaxies were selected. Here we describe the proper way to derive density fields from galaxy redshift surveys. We limit ourselves to measuring the density in redshift space, ignoring the effects of deviations from the Hubble law due to galaxy peculiar velocities. The subject of galaxy density fields dates back to Ref. [9]. An educational recent review is that of Ref. [10].

Our results will be based on two surveys. First, we consider the Center for Astrophysics Redshift Survey (CfA2; [12]). This survey comprises about 10,000 galaxy redshifts, selected to be brighter than  $m = 15.5$ , (approximately, a  $B$ -band magnitude). It covers an area which is about 17% of the whole sky. However, in order to evaluate the effects of the density field of galaxies on the cosmic ray spectrum, we really should probe the density field over nearly the whole sky. The best sample of galaxies to use for this purpose is the IRAS PSCz Survey [13], which consists of about 15,000 galaxies with infrared fluxes  $> 0.6$  Jy over about 84% of the sky.

A consequence of the flux limits in any survey is that at different redshifts, a different set of galaxy luminosities  $L$  is observed, determined by the faintest luminosity observable at that redshift  $L_{\min}(z)$ . For an Euclidean metric, this luminosity is related to the flux limit by  $L_{\min}(z) = 4\pi(H_0 cz)^2 f_{\text{lim}}$ .

If the distribution of galaxy luminosities is described by the galaxy luminosity function  $\Phi(L)$ , it is then simple to calculate what fraction of all galaxies is observable at any redshift:

$$\phi(z) = \frac{\int_{L_{\min}(z)}^{\infty} dL \Phi(L)}{\int_0^{\infty} dL \Phi(L)}. \quad (1)$$

The quantity  $\phi(z)$  is usually referred to in the literature as the “selection function” [14]. The most common methods used to determine the galaxy luminosity function from the survey itself are those of [15] and [16]. These methods assume that the luminosity function has universal shape, but *not* that galaxies are distributed homogeneously.

Figure 1 shows in the top panel the distribution of galaxies and redshifts in CfA2. Here we express galaxy luminosity in terms of the “absolute magnitude”  $M = -2.5 \log_{10} L + \text{const}$ . The thick solid line shows the flux limit of the survey, translated into an absolute magnitude limit at each redshift. Because of this limit a number of galaxies which are observable at low redshifts are too faint to be observed at higher redshift.

The fraction of galaxies  $\phi(z)$  between absolute magnitudes  $-22 < M < -10$  which are unobservable at each redshift is shown in the bottom panel of Figure 1, based on a fit to the luminosity function in the survey using the method of [15]. Because the function falls rapidly from unity, it is clear that even at low redshifts the effects of the flux limit are important. We can use  $\phi(z)$  to calculate the expected distribution of observed galaxies with redshift. The top panel of Figure 2 compares these expected counts (dotted line) in redshift shells of thickness 0.001

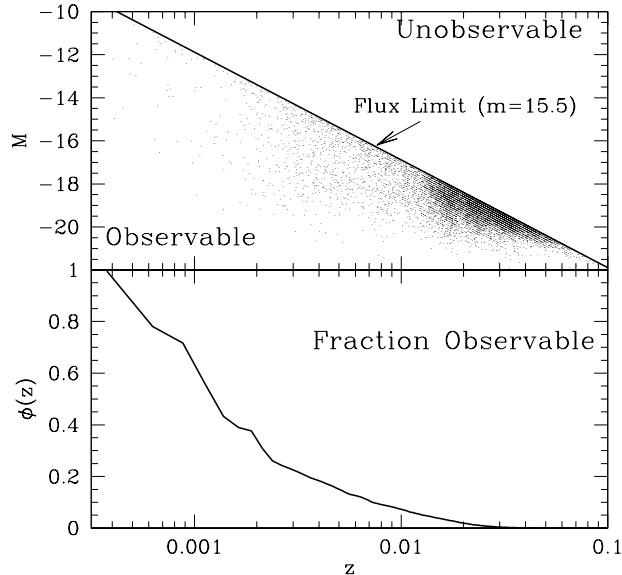


**FIGURE 1.** The top panel shows the absolute magnitudes (related to luminosity by  $M = -2.5 \log_{10} L + \text{const}$ ) and redshifts of CfA2 galaxies. Shown as the thick solid line is the flux limit, converted to the appropriate absolute magnitude at each redshift. The bottom panel shows the fraction of galaxies in the range  $-22 < M < -10$  that we estimate to be brighter than the flux limit. This function falls rapidly with redshift. When interpreting the top plot, remember that the volume probed at low redshift is far smaller than that probed at high redshift.

to the observed counts (solid line) in CfA2. It appears that locally we are in an overdensity of galaxies of about a factor of two; note that at large distances, where each shell corresponds to a considerable amount of volume, the number of galaxies is very nearly the expected number.

If the flux limits are ignored, as in [11], the incorrect conclusion that we live in a large overdensity is easily recovered (dashed lines in Fig. 2).

As mentioned above, the CfA2 survey covers a relatively small fraction of the sky. Thus, the PSCz redshift survey provides a more useful sample to use in the context of this paper. Using the selection function provided by [13], we again show the expected versus the observed counts for the PSCz survey in the bottom panel of Figure 2. This survey also shows we are living in a slight overdensity, and furthermore reveals the general homogeneity of the nearby universe. (The actual counts and their dependence on redshift are slightly different than for CfA2, because the galaxies are selected in different ways).

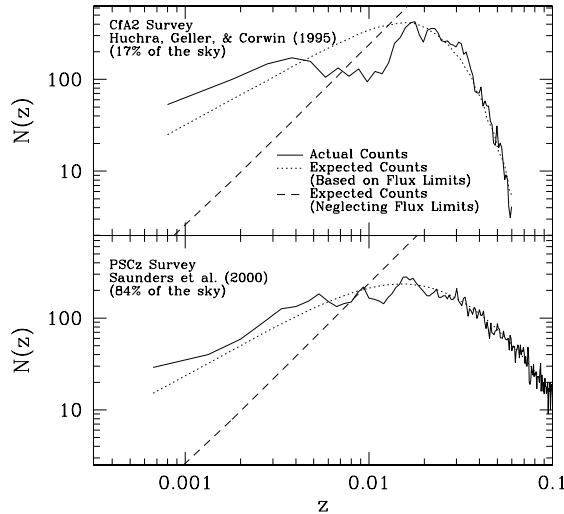


**FIGURE 2.** Comparison of observed counts (solid line) to those predicted based on the flux limits (dotted line) and those predicted neglecting the flux limits (dashed line). The CfA2 survey is shown at top, the PSCz at bottom. Both show a local overdensity of only about a factor of two when the flux limits are properly accounted for.

## CALCULATION OF THE DIFFUSE FLUX OF UHECRS

We calculate the diffuse flux of UHECR protons numerically and compare our results with the analytical calculations carried out as in [17]. Our propagation code includes pair production and photopion production as energy losses and also adiabatic energy losses due to the expansion of the universe. Since the inelasticity for pair production is very low, we consider it as a continuous energy loss process. The magnetic field is not included. A more detailed description of the numerical approach and of the results is reported in [8].

In order to compare the results of the simulation with the observed statistics of events of operating or planned detectors, we generate the events in such a way that the total number of events above  $10^{19}$  eV equals the observed number for the specific experiment under consideration.

The results of the code are checked versus the analytical results for the modification factor from single sources and from a diffuse distribution of sources. The agreement is excellent, and the effect of the fluctuations at energies larger than  $\sim (3 - 4) \times 10^{19}$  eV is evident (see below). On average the simulated flux is slightly larger than the analytical one, as expected on the basis of the stochasticity of the process of photopion production (on small distances there is an appreciable chance that some protons do not interact at all).

We investigate the effects of the *real* distribution of sources on the observed

spectra of UHECRs, for different choices of the injection spectrum.

The possibility that a local overdensity of sources of UHECRs may help in solving the problem of the existence of events above the GZK cutoff goes back to [3] and is summarized in [18]. The effect can easily be understood, since the severe photopion energy losses limit the maximum distance of UHECRs to distances of a few Mpc, while lower energy CRs can come from much larger distances. A local overdensity mainly affects, as a consequence, the fluxes of UHECRs. This is illustrated in Fig. 3 for a toy model in which the local overdensity is a top-hat function with  $\Delta\rho/\rho = 1, 10, 30$  (solid, dashed and dash-dotted lines respectively) in a region of  $\sim 20$  Mpc around the Earth. The fluxes of UHECRs have been calculated following the analytical approach of [17].

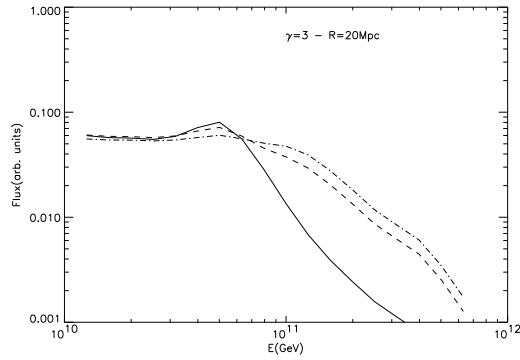


**FIGURE 3.** *The effect of a local overdensity within 20 Mpc on the fluxes of UHECRs.*

In order to have a direct comparison with the results of Ref. [11], we first consider the case of an injection spectrum  $E^{-\gamma}$  with  $\gamma = 3$  and a source distribution extended up to a maximum redshift  $z_{max} = 0.1$ , that corresponds approximately to the maximum redshift available in the PSCz catalog. It is worth stressing that the reason for the choice  $\gamma = 3$  in [11] was motivated by the need to first reproduce the results of Yoshida and Teshima [19], whose curve is usually superimposed to the AGASA results [20]. However, that curve seems to be obtained for  $\gamma = 2.3$  (Teshima, personal communication). The results of our calculations and of Ref. [11] seem to be incompatible with such a choice of the power index.

We carry out the simulation for a homogeneous distribution of the sources and then for a source distribution that follows the profile found in the previous section, after the correction for selection effects.

The generation of events is ended when the total number of events with energy above some threshold equals the observed number. In fig. 4 we normalize the flux at  $10^{19}$  eV and we stop the generation of new events when the total number of events above  $10^{19}$  eV becomes  $728^1$ , equal to the number of events detected by

<sup>1)</sup> This sample includes the newly released AGASA data [21]

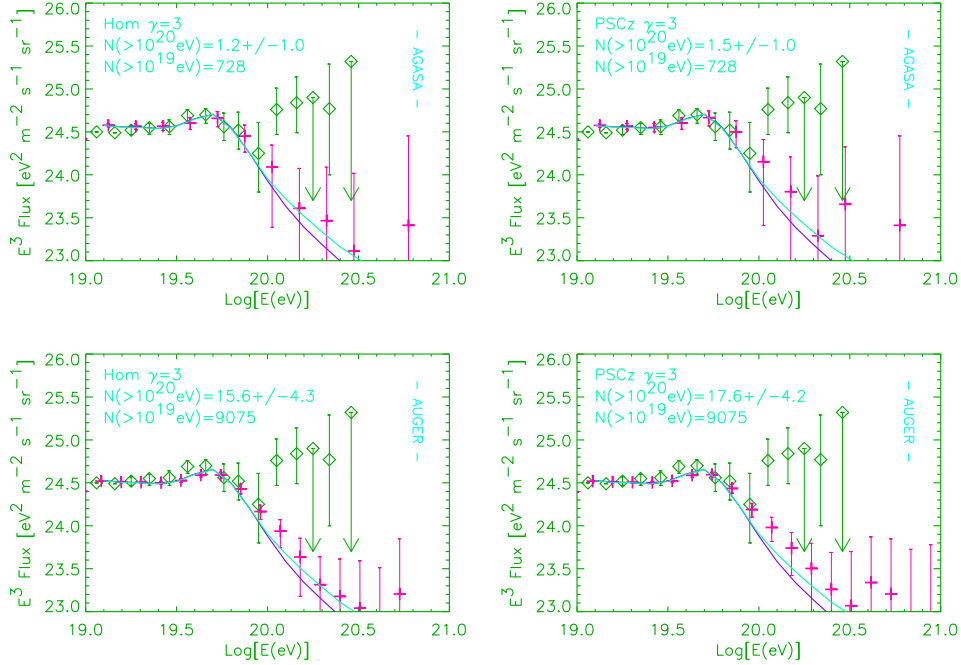


**FIGURE 4.** Results of the simulations for an injection spectrum  $E^{-3}$ . In the four panels the dark and light continuous lines are the result of the analytical calculations for the homogeneous distribution of sources and for a distribution following the PSCz catalog. The diamonds are the AGASA data. Upper left: homogeneous distribution and  $N(> 10^{19} \text{eV})=728$ ; upper right: PSCz catalog and  $N(> 10^{19} \text{eV})=728$ ; lower left: homogeneous distribution and  $N(> 10^{19} \text{eV})=9075$ ; lower right: PSCz catalog and  $N(> 10^{19} \text{eV})=9075$ .

AGASA in that energy range. The left upper panel is for a homogeneous distribution of the sources, while the right upper panel is obtained by adopting the PSCz distribution of galaxies. The diamonds are the AGASA data points and the crosses are the results of the simulation. The error bars in the simulation are obtained by generating 100 realizations and calculating their mean and variance. The continuous curves represent the result of the analytical calculation for the same value of the parameters. The lower curve is for the homogeneous case and the upper curve for the distribution derived from the PSCz catalog. One can easily see that the difference is small, which is expected since the correction for selection effects considerably reduces the local overdensity in comparison to what found by [11]. The total number of events with  $E > 10^{20} \text{eV}$  is  $1.2 \pm 1.0$  for the homogeneous case and  $1.5 \pm 1.0$  for the PSCz catalog galaxies. No one of our realizations had a number of events above  $10^{20} \text{eV}$  comparable with observations. The main reason for that is that the spectrum is quite steep, in addition to the suppression due to photopion production.

In order to study the effect of an increased statistics of events, we simulated the

situation for the case of Auger (9075 events predicted above  $10^{19}$  eV in the first 3 years of operation). The situation is illustrated in the two lower panels of fig. 4 (on the left the homogeneous case and on the right the PSCz case). In general, the size of the error bars decreases everywhere. The number of events at  $E > 10^{20}$  eV (see figures) in the two cases is still much smaller than the projected one ( $\sim 100$ ).

Since the main reason for the small number of events at high energy in the simulations is the steep spectra adopted above and in [11], it is natural to look for different choices.

Many acceleration mechanisms produce spectra which are quite flatter than  $E^{-3}$ . We calculate the expected flux of UHECRs for an injection spectrum  $E^{-2.1}$ . In this case the normalization is chosen in such a way that the total number of events with energy  $E > 4 \times 10^{19}$  eV is the same as observed by AGASA (49 events). The reason for this normalization will be clear below.

The results of the simulation and the corresponding analytical result are plotted in fig. 5 for three cases: homogeneous distribution of the sources with  $z_{max} = 0.1$  (crosses), PSCz distribution with  $z_{max} = 0.1$  (stars), homogeneous distribution with  $z_{max} = 1$  (squares).

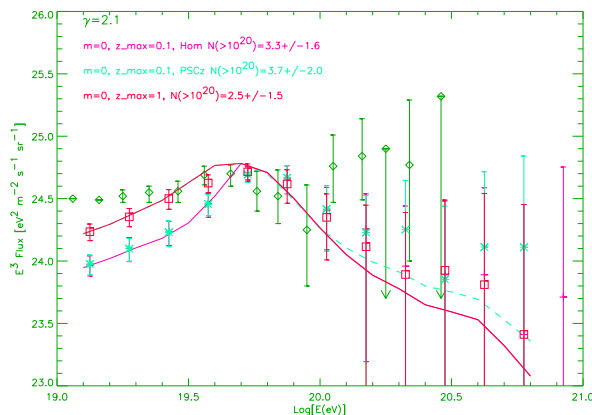


**FIGURE 5.** UHECRs from an injection spectrum  $E^{-2.1}$ . The diamonds are the AGASA data. The results of the simulation are for an homogeneous distribution and  $z_{max} = 0.1$  (crosses), for the PSCz sources and  $z_{max} = 0.1$  (stars) and for an homogeneous distribution and  $z_{max} = 1$  (squares). The continuous lines are the analytical results for the same cases.

The number of events at  $E > 10^{20}$  eV is mainly determined by the local distribution of the sources. For the adopted normalization, the homogeneous distribution gives  $3.3 \pm 1.6$  events above  $10^{20}$  eV (to be compared with 8) and the PSCz distribution provides  $3.7 \pm 2.0$  events in the same range. In this last case, about 5% of our realizations give a number of events above  $10^{20}$  eV which is equal to or larger than the observed one. <sup>2</sup> The conclusion that the number of events above  $10^{20}$

<sup>2</sup>) If the old AGASA statistics of 47 events above  $4 \times 10^{19}$  eV is used, 15% of the realizations give a number of events above  $10^{20}$  eV equal to or larger than the 6 observed then.



eV is within  $\sim 2$  sigmas of the observations for an injection spectrum  $\sim E^{-2}$  is consistent with the findings in [22].

The deficit of events at energies lower than  $\sim (3 - 4) \times 10^{19}$  eV is evident in the case  $z_{max} = 0.1$ . The high redshift sources only contribute additional flux at the low energies, therefore we also considered the case  $z_{max} = 1$ . From fig. 5 it appears that the deficit is now evident only at energies lower than  $\sim 2 \times 10^{19}$  eV, where additional factors might further improve the low energy agreement. Some possible factors are: 1) cosmological magnetic fields; 2) source evolution; 3) a separate (possibly galactic) component which is relevant at lower energies and has a steep spectrum. These possibilities are discussed at length in [8].

## SUPER HEAVY DARK MATTER: THE DIRECT CONNECTION

In this section we consider another example of a possible connection between the problem of the dark matter and the explanation of the UHECRs.

Heavy particles ( $m_X \sim 10^{12} - 10^{14}$  GeV) can be produced in the Early Universe in different ways [4–7] and their lifetime can be finite though very long compared to the present age of the universe. In these circumstances, super-heavy particles can represent an appreciable fraction, if not all of the cold dark matter in the universe [4–7]. The occasional decay of these particles results in the production of UHECRs, as widely discussed in the literature [5,23–25]. In particular, if the relics cluster in galactic halos, as is expected, they can explain the cosmic ray observations above  $\sim 5 \times 10^{19}$  eV.

The decay of heavy relics results usually in the production of a quark-antiquark pair which rapidly hadronizes, generating two jets with approximately 95% of the energy in pions, and  $\sim 5\%$  in baryons. The decay of the pions results in the observed high energy particles, mainly in the form of gamma rays, and in the generation of ultra-high energy neutrinos. The spectrum of the gamma photons is relatively flat ( $\sim E^{-1.5}$ ) reflecting the behaviour of the fragmentation function for the quarks. Therefore two main signatures of this model are: *i*) a flat energy spectrum; *ii*) composition dominated by gamma rays rather than by protons. Moreover, as in all top-down models, heavy elements are expected to be completely absent. Several calculations of the expected fluxes have been performed and presented in the literature. In Fig. 6 we report the results of the calculations of Ref. [25]. The solid curves in fig. 6 are obtained by using a supersymmetric generalization of the quark fragmentation function, derived in [26], while the dashed lines are obtained by using the standard MLLA-QCD fragmentation function [27]. The thick lines are for  $m_X = 10^{14}$  GeV, while the thin lines are for  $m_X = 10^{13}$  GeV.

In [28,24] it was first recognized that, due to the asymmetric position of the Earth in the Galaxy, an appreciable anisotropy would result in this model. In [29,30] this issue was considered more quantitatively, taking into account the exposure of the present experiments. All authors concur that the present data is consistent with

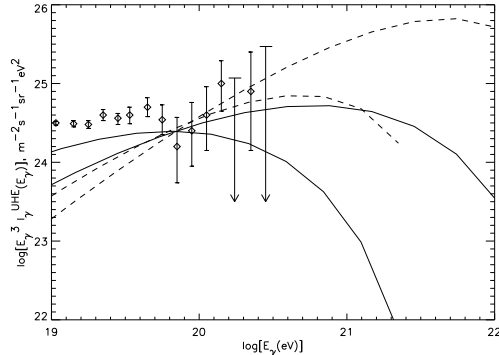


**FIGURE 6.** Fluxes of UHECRs from SH relics.

the predictions of the relic model for practically all reasonable values of the model parameters.

Recently, an interesting pattern has arisen from the analysis of the events with energy larger than  $4 \times 10^{19}$  eV: in [20] the sample with this energy cut comprises 47 events<sup>3</sup>, whose overall distribution in space does not show appreciable deviation from isotropy. However, 3 doublets and one triplet were identified within an angular scale of  $2.5^\circ$ , comparable with the angular resolution of the experiment. A complete analysis, including the whole set of UHECR events above  $4 \times 10^{19}$  eV from the existing experiments was performed in [31]. This extended sample comprises 92 events and shows 12 doublets and two triplets (each triplet is also counted as three doublets) within an angle of  $3^\circ$ . The chance probability of having more than this number of doublets was estimated to be  $\sim 1.5\%$ . Although it is probably too soon to rule out the possibility that these multiplets are just a random fluctuation, it is instructive to think about the possibility that their presence contains some physical information about the sources of UHECRs. Most of the top-down models for UHECRs (e.g. strings, necklaces, vortons, etc.) cannot naturally explain the multiplets.

Here we discuss how the multiplets can be interpreted in the context of the super-heavy dark matter (SHDM) model, following the discussion in [32]

We know a few things on dark matter, mainly as suggested by N-body simulations (see for instance [33]). Dark matter seems to be clustered in galactic halos with a distribution strongly peaked in the center. We model this distribution as in [34]:

$$n_H(r) = n^0 \frac{(r/r_c)^{-1}}{\left[1 + \frac{r}{r_c}\right]^2}, \quad (2)$$

where  $r_c$  is the core size and  $n^0$  is a normalization parameter. These two parameters can be set by requiring that the halo contains a given total mass ( $M_H$ ) and that the

<sup>3</sup>) The data in [21] were not included in this analysis.

velocity dispersion at some distance from the center is known (in the case of the Galaxy, the velocity dispersion is  $\sim 200$  km/s in the vicinity of our solar system.). Alternative fits to the simulated dark matter halos and a discussion of whether or not simulated halos appear to be consistent with observations are provided in [33].

In addition to the smooth dark matter distribution, represented by eq. (2), N-body simulations also show that there is a clumped component which contains  $\sim 10-20\%$  of the total mass. The presence of these clumps are a natural consequence of the way in which gravity assembles dense virialized halos such as our galaxy today from the initially smooth density fluctuation field which was present when the cosmic microwave background (CMB) decoupled from the baryons. A more extended discussion on the formation and merging of the clumps can be found in [32] and references therein.

We found that a good fit to the joint distribution in clump mass and position in the simulations of [33] is given by

$$n_{cl}(r, m) = n_{cl}^0 \left( \frac{m}{M_H} \right)^{-\alpha} \left[ 1 + \left( \frac{r}{r_c^{cl}} \right)^2 \right]^{-3/2}, \quad (3)$$

where  $n_{cl}^0$  is a normalization constant,  $r_c^{cl}$  is the core of the clumps distribution, and  $\alpha$  describes the relative numbers of massive to less massive clumps. The simulations suggest that  $\alpha \sim 1.9$  [33]. The constraints on the core size are weaker—we will study the range where  $r_c^{cl}$  is between 3 and 30 percent of  $R_H$ . In [33], a halo with  $M_H \approx 2 \times 10^{12} M_\odot$  contains about 500 clumps with mass larger than  $\sim 10^8 M_\odot$ . This sets the normalization constant in eq. (3).

Clumps in the parent NFW halo are truncated at their tidal radii. The tidal radius of a clump depends on the clump mass, the density profile within the clump, and on how closely to the halo center it may have been. We assume that clumps of all mass are isothermal spheres (even though they are not truly isothermal, [33] suggest this is reasonably accurate):  $\rho_{cl}(r_{cl}) \propto 1/r_{cl}^2$ , where  $r_{cl}$  is the radial coordinate measured from the center of the clump.

As shown in [24,30], the total (energy integrated) flux of UHECRs per unit solid angle from a smooth distribution of dark matter particles in the halo is  $\frac{d\Phi}{d\Omega} \propto \int_0^{R_{max}} dR n_H(r(R))$ , where  $R$  is the distance from the detector, and  $r$  is the distance from the galactic center (so  $R$  and  $r$  are related by trigonometrical relations accounting for the off-center position of the Earth in the Galaxy). The upper limit,  $R_{max}$ , depends on the line of sight.

It is intuitively obvious that clumped regions will give an excess of events from certain directions, as was first pointed out in [35]. Details of the numerical calculation of the fluxes and direction of arrivals of UHECRs can be found in [32].

Fig. 7 shows as an example one of the generated flux maps: the map represents the ratio of the total flux including the contribution from clumps, to the flux obtained by using a smooth NFW profile. The various free parameters were  $r_c = 8$  kpc,  $r_c^{cl} = 10$  kpc, and the mass distribution was truncated at a clump mass of 1% of the mass of the NFW halo. This sort of plot emphasizes the clump contribution.

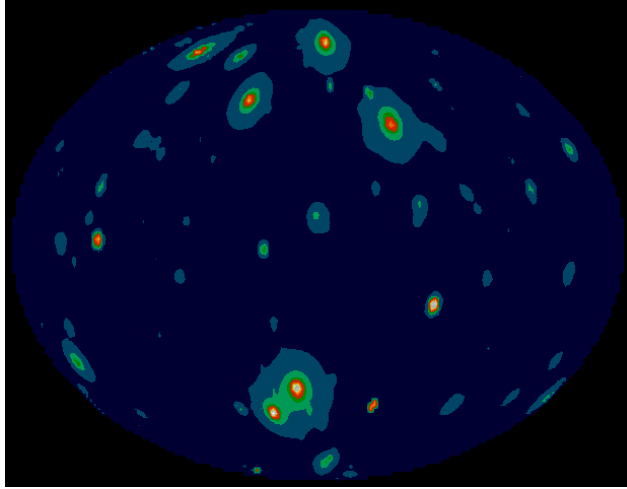


**FIGURE 7.** *Small scale anisotropies in the model of super-heavy relics in the halo.*

To calculate the small scale anisotropies, we generated  $10^4$  mock samples, each of 92 observed events, and counted the number of doublets and triplets for angular scales of 3, 4, and 5 degrees. Our codes can also be used to check the corresponding numbers for the case of isotropic arrival directions (as in [31]). Two sets of values of the cores for the NFW and the clumped component were adopted, one in which  $r_c = 8$  kpc and  $r_c^{cl} = 10$  kpc (case 1) and the other with  $r_c = r_c^{cl} = 20$  kpc (case 2). The observed numbers of doublets within 3, 4, and 5 degrees for an isotropic distribution of arrival directions are given in [31] and are 12, 14 and 20 respectively. The number of doublets that we obtain in case 1 are 8, 14, and 21 within 3, 4, and 5 degrees respectively. The probability that the number of doublets equals or exceeds that observed is 12%, 47% and 57% respectively. This should be compared with the 1.5%, 13.4% and 15.9% quoted in [31] for an isotropic distribution of arrival directions.

We repeated the same calculation for the case 2. The corresponding averages and probabilities of exceeding the observed number of doublets within 3, 4 and 5 degree scales are 6.6, 12, and 18, and 4.5%, 29% and 36% respectively.

In both cases 1 and 2, the number of doublets on angular scales of 4 and 5 degrees is consistent with the observed values; presumably the discrepancy at 3 degrees is random chance.

We have also studied the occurrence of triplets. There is some ambiguity as to how a triplet is best defined; we have chosen to define triplets as configurations in which all three pairs would have been classified as doublets. (This means, for example, that a co-linear configuration of two doublets is not necessarily a triplet.) With this definition, the average number of triplets in case one is 0.5, 1.5 and 3, with the probability of having more than the observed triplets (2, 2, 3 respectively) equal to 4%, 16% and 35%. For case 2, the correspondent numbers are 0.4, 1, and

2.5 triplets and 2%, 8% and 20% for the probabilities to have more triplets than observed.

It is instructive to explore the reasons for the multiple events in the SHDM model. If we study the case in which all the halo mass is in the smooth NFW component, then the number of doublets typically drops by one or two. This suggests that the anisotropy due to our position in an NFW halo can result in a number of multiplets of events which is considerably larger than if the arrivals were from an isotropic background. The number of multiplets from the clumped component is mainly affected by the presence of large nearby clumps, whose number depends on the high mass cutoff imposed in the mass function of clumps. A maximum mass of 1% of the halo mass implies a total mass in the clumps of  $\sim 10 - 15\%$  of  $M_H$ , consistent with the results of the simulations [33]. Larger cutoffs imply larger mass fractions, which are harder to reconcile with the N-body simulations.

## CONCLUSIONS

We discussed here two possible connections between the problem of origin and clustering properties of dark matter and the nature of the particles with energy in excess of  $10^{20}$  eV.

In the first part we investigated an indirect connection, consistent in the effect on the fluxes of UHECRs due to local clustering of the sources, driven by the corresponding clustering of dark matter. It has been known for a long time [3,18] that a local overdensity in the sources of UHECRs may shift the energy of the GZK cutoff towards larger energies. The overdensities needed to make this effect relevant as a possible solution of the UHECR puzzle are of the order of  $\sim 10$  or more. In a recent paper, Medina-Tanco [11] claimed that this is exactly the value extracted from large scale structure surveys like the CfA2 catalog. We reconsidered this problem and showed that, by correctly extracting the density field from the CfA2 and the PSCz catalogs, the local overdensity is not larger than  $\sim 2$ , so that the calculations of the propagation of UHECRs are not particularly affected by the local source distribution. In other words the increase in the number of events above  $10^{20}$  eV, in comparison with the case of homogeneous distribution is not important [8].

On the other hand we noticed an interesting point: using an injection spectrum  $E^{-2.1}$  typical of astrophysical sources, we obtain a number of events with energy above  $10^{20}$  eV, which is basically compatible with the observed number, once the statistical fluctuations and the Poisson noise in the photopion production have been taken into account. The agreement of the prediction at lower energies, depend on additional physics (evolution of the sources, cosmological magnetic fields or an additional (possibly) galactic component at energies around  $(1 - 2) \times 10^{19}$  eV) that was not included in our calculations.

In the second part of the paper, we investigated a direct connection between dark matter and UHECRs. It has been proposed that most of the dark matter

might be made of super heavy quasi-stable particles, created in the early universe. These particles would cluster in large scale structures, and in particular in the galactic halo. The rare decays of the super heavy dark matter particles in the halo can easily explain the fluxes of UHECRs that are observed. We reviewed the testable predictions of this model and then concentrated on a particular aspect, the anisotropy of arrival directions. A large scale (dipole) anisotropy in this model is easily foreseeable, since the earth is off center in the Galaxy. The predicted large scale anisotropy is compatible with the observed one [29,30], mainly due to a lack of exposure in the direction of the galactic center. Based on the clustering properties of dark matter on smaller scales, we also discussed the recent results of [32] on the the small scale anisotropies. Based on the informations provided by N-body simulations of structure formation, the combination of the smooth peculiar density profile in the Galaxy and the clumped component survived in the halo can explain the observed small scale anisotropies, in terms of doublets and triplets of events. Future full sky experiments as Auger [36] will be extremely important to test this model, mainly in two ways: 1) an increased statistics of events will allow a better determination of the small angle clustering, and 2) a better composition determination will definitely allow to understand if gamma rays are an important component of the UHECRs.

**Aknowledgments** I am grateful to my collaborators, M. Blanton, A.V. Olinto and R.K. Sheth, for continuos interactions. I am also grateful to the organizers of the “International Workshop on Observing UHECRs from Space and Earth” for the nice environment that allowed instructive discussions with P. Biermann, J. Ellis, T. Gaisser, D. Harari, A. Letessier-Selvon, J. Linsley, L. Scarsi, G. Sigl, M. Teshima and T. Weyler among others. This work was supported by the DOE and the NASA grant NAG 5-7092 at Fermilab.

## REFERENCES

1. Greisen, K., *Phys. Rev. Lett.* **16**, 748 (1966).
2. Zatsepin, G. T., and Kuzmin, V. A., *Pis'ma Zh. Eksp. Teor. Fiz.* **4**, 114 (1966) [*JETP Lett.* **4**, 78 (1966)].
3. Berezhinsky, V. S., and Grigorieva, S. I., *Proc. 16th. Int. Cosmic Ray Conf., Kyoto* **2**, 81 (1979).
4. Chung, D. J. H., Kolb, E. W., and Riotto, A., *Phys. Rev. Lett.* **81**, 4048 (1998).
5. Berezhinsky, V. S., Kachelriess, M., and Vilenkin, A., *Phys. Rev. Lett.* **79** 4302 (1997).
6. Kuzmin, V. A., presented at the Workshop “Beyond the Desert”, Castle Ringberg, 1997, astro-ph/9709187; International Workshop on Non-Accelerator New Physics, Dubna, 1997.
7. Kuzmin, V. A. and Tkachev, I. I., preprint astro-ph/9903542.
8. Blanton, M., Blasi, P., and Olinto, A. V., in preparation.
9. Davis, M., & Huchra, J., *Astrophys. J.* 254, 437 (1982).
10. Strauss, M. A., & Willick, J.A., *Phys. Rep.* 261, 271 (1995).
11. Medina Tanco, G. A., *Astrophys. J.* **510**, 91 (1999).

12. Huchra, J. P., Geller, M. J., & Corwin, Jr., H. G., *Astrophys. J. Suppl.* **70**, 687 (1995).
13. Saunders, W., Sutherland, W. J., Maddox, S. J., Keeble, O., Oliver, S. J., Rowan-Robinson, M., McMahon, R. G., Efstathiou, G., Tadros, H., White, S. D. M., Frenk, C. S., Carraminana, A., Hawkins, M. R. S., submitted to *MNRAS*, preprint (astro-ph/0001117).
14. Peebles, P. J. E., *The Large-Scale Structure of the Universe* (Princeton, NJ: Princeton University Press) 1990.
15. Efstathiou, G., Ellis, R. S., & Peterson, B. S., *MNRAS* **232**, 431 (1988).
16. Sandage, A., Tammann, G. A., & Yahil, A., *Astrophys. J.* **232**, 352 (1979).
17. Berezhinsky, V. S., and Grigorieva, S. I., *Astron. Atroph.* **199**, 1 (1988).
18. Berezhinsky, V. S., et al. *Astrophysics of cosmic rays*, Amsterdam: North-Holland, 1990, edited by Ginzburg, V.L.
19. Yoshida, S., and Teshima, M., *Prog. Theor. Phys.* **89**, 833 (1993).
20. Takeda, M., et al., *Phys. Rev. Lett.* **81**, 1163 (1998).
21. Hayashida, N., et al., Appendix to *Astrophys. J.* **522**, 225 (1999) (preprint astro-ph/0008102).
22. Bahcall, J. N., and Waxman, E., to appear in *Astrophys. J.* (preprint hep-ph/9912326).
23. Birkel, M., and Sarkar, S., *Astropart. Phys.* **9**, 297 (1998).
24. Berezhinsky, V. S., Blasi, P., and Vilenkin, A., *Phys. Rev.* **D58**, 103515 (1998).
25. Blasi, P., *Phys. Rev.* **D60**, 023514 (1999).
26. Berezhinsky, V. S., and Kachelriess, M., *Phys. Lett.* **B434**, 61 (1998).
27. Dokshitzer, Yu. L., et al., *Basics of Perturbative QCD*, Editiones Frontières, Gif-sur-Yvette, France, 1991.
28. Dubovsky, S. L., and Tynyakov, P. G., *Pis'ma Zh. Eksp. Teor. Fiz.* **68**, 99 (1998) [*JETP Lett.* **68**, 107 (1998)].
29. Berezhinsky V. S., and Mikhailov, A., *Phys. Lett.* **B449**, 237 (1999).
30. Medina Tanco G. A., and Watson, A. A., *Astropart. Phys.* **12**, 25 (1999).
31. Uchihori, Y., et al., *Astropart. Phys.* **13**, 151 (2000).
32. Blasi, P., and Sheth, R. K., *Phys. Lett.* **B486**, 233 (2000).
33. Ghigna, S., Moore, B., Governato, F., Lake, G., Quinn, T., Stadel, J., preprint astro-ph/9910166; Moore, B., Ghigna, S., Governato, F., Lake, G., Quinn, T., Stadel, J., Tozzi, P., *Astrophys. J.* **524**, 19 (1999); Tormen, G., Diaferio, A., Syer, D., *MNRAS* **299**, 728 (1998).
34. Navarro, J. F., Frenk, C. S., and White, S. D. M., *Astrophys. J.* **462**, 563 (1996).
35. Berezhinsky, V., Invited talk at TAUP-99, Paris, September 6 - 10, 1999, preprint hep-ph/0001163.
36. Cronin, J. W., *Rev. Mod. Physics* **71**, 175 (1999).